JOURNAL OF MATERIALS SCIENCE 32 (1997) 3435–3442

Electron back scattered diffraction (EBSD) analysis of quasi-cleavage and hydrogen induced fractures under cyclic and dwell loading in titanium alloys

M. R. BACHE, W. J. EVANS, H. M. DAVIES
Interdisciplinary Research Centre in Materials for High Performance Applications, University of Wales, Swansea, SA2 8PP, UK

Evidence for sub-surface fatigue crack initiation is often reported for near alpha titanium alloys such as the coarse grained IMI685 and the fine duplex structured IMI834. In such materials with a typical as received hydrogen concentration of 40–60 ppm the initiation site is invariably characterized by quasi-cleavage facetting. Similar facetting is also associated with the low temperature dwell sensitive fatigue response in the same alloys. For IMI685, it is reported that this failure mechanism is replaced by α/β interface cracking when the alloy contains a relatively high concentration of interstitial hydrogen. The present paper characterises the local grain orientation and microstructural conditions associated with these various forms of failure through the use of a microtextural analysis technique based upon electron back scattered diffraction (EBSD) measurements. The observations are related to an existing model to account for facet formation based upon the pile-up of dislocations at grain-boundaries. The implications for further use of this technique with titanium alloys are discussed.

1. Introduction

Sub-surface fatigue crack initiation is commonly reported for titanium alloys [1]. In the near alpha systems containing typical as received hydrogen levels of about 60 ppm, such sites are invariably characterized by quasi-cleavage facets which have been shown to be of near basal orientation with respect to the hexagonal crystal lattice [2]. It is reported, however, that alloys with a relatively high concentration of interstitial hydrogen (> 100 ppm) fail by a different fracture mechanism in which initiation and growth along α/β plate interfaces becomes dominant [3]. Clearly, the requirement to combine initiation based lifing technology with damage tolerant criteria requires a better understanding of these failure processes and the localized conditions necessary for subsequent crack growth. In addition, clarification of the mechanisms for facet formation will allow modifications to the alloy processing route so that, for instance, advantageous microstructural textures may then be introduced as a means of enhancing the component fatigue performance.

The present paper sets out to characterize quasi-cleavage facets formed under fatigue loading conditions in two near alpha titanium alloys with distinctly different microstructures. One alloy, IMI834 (Ti–5.8Al–4Sn–3.5Zr–0.7Nb–0.5Mo–0.35Si–0.06C wt %), has a fine duplex morphology while the other, IMI685 (Ti–6Al–5Zr–0.5Mo–0.25Si wt %), has a much coarser lamellar form. The analysis uses back scattered electron diffraction (EBSD) techniques to evaluate the crystallographic orientation of specific grains or alpha colonies in the alloy microstructure. It relies on the recognition of X-ray diffraction patterns (Kikuchi patterns) obtained from back scattered electrons generated by the localized interaction of a primary electron beam and a steeply inclined specimen surface. In the case of the titanium alloys, the orientation of the basal plane with respect to fracture surface features and stress biaxiality is of particular interest.

The fatigue failures were generated in laboratory test pieces machined from the IMI685 and IMI834. The IMI685 was tested in the coarse aligned microstructural condition containing either an as received hydrogen concentration of 60 ppm or a modified level of 250 ppm. Both cyclic and dwell fatigue under tension and torsion loading modes were evaluated. This alloy was considered as a suitable vehicle for the assessment of the EBSD technique due to its relatively large prior beta grain size and the resultant large scale facets that form under fatigue. The IMI834 has a much finer grain structure which is bi-modal in character. Under fatigue loading it shows a strong tendency to develop sub-surface facets. Clearly, it is necessary to identify the nature of these particularly since the alloy has been found to behave differently from IMI685 under biaxial loading conditions [4]. The as received hydrogen content of the IMI834 was 40 ppm.

0022–2461

Optical and scanning electron microscopy studies of the fracture surfaces were used to arrive at an initial selection of typical fracture morphologies from the range of alloy conditions evaluated. It is demonstrated that EBSD has provided important information concerning the crystallographic orientation of facets and the local orientation of grains immediately surrounding initiation sites. The measurements lend support to a model for facet formation previously proposed by Evans and Bache based on dislocation pile-ups [1].

2. Experimental methods

2.1. Fatigue failures

Specimens were manufactured from IMI685 and IMI834, both supplied in the form of 30 mm round bar. In the case of IMI685, the as received alloy contained a hydrogen concentration of 60 ppm. Selected specimen blanks were degassed by vacuum annealing at 800 °C for 18 h and subsequently recharged to a relatively high hydrogen content of 250 ppm using a hydrogenation technique previously reported [3]. Finally, each blank was solution heat treated in air above the beta transus (1030 °C) for 45 min followed by furnace cooling to laboratory temperature and aging at 550 °C for 24 h. This produced a coarse aligned microstructure of transformed alpha plates with a small amount of retained beta at the lath boundaries, Fig. 1. The IMI834 was evaluated with an as received hydrogen level of 40 ppm. It was heat treated to give a retained primary alpha content of 15%. This was achieved by heating in the alpha + beta field (1025 °C) for 2 h followed by oil quenching and a 2 h age at 700 °C. The fine grained "bi-modal" microstructure shown in Fig. 2 was obtained with primary alpha and matrix grain diameters of approximately 20 μm and 60 μm respectively.

Fatigue testing was conducted at ambient temperature on a closed loop servo-hydraulic machine with a maximum load and torque capacity of 50 KN and 400 Nm. The tubular specimen design illustrated in Fig. 3 was used for IMI685 whereas the solid, plain cylindrical testpiece in Fig. 4 formed the basis of the work on IMI834. "Cyclic" and "dwell" loading waveforms are represented schematically in Fig. 5. The former incorporated a 2 s rise and fall between peak and minimum stress with a 1 s hold at peak load to facilitate data acquisition. The latter had the same rise and fall times but included a 120 s dwell at peak load. All fatigue loading involved an R ratio of 0.1.

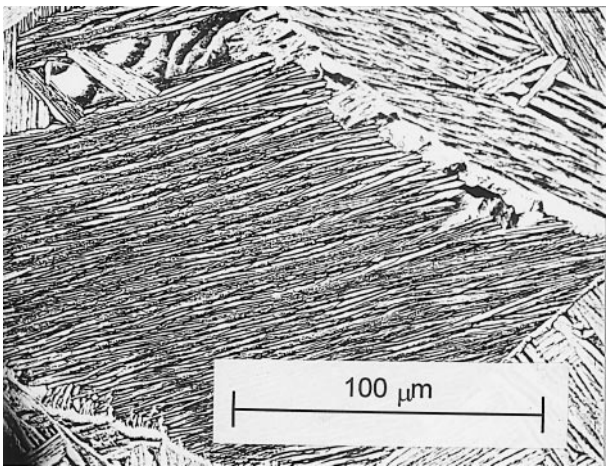

Figure 1 Aligned microstructure in IMI685.

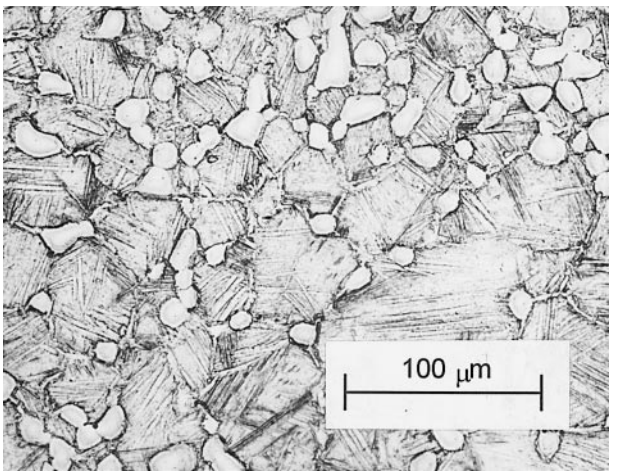

Figure 2 Bi-modal microstructure in IMI834.

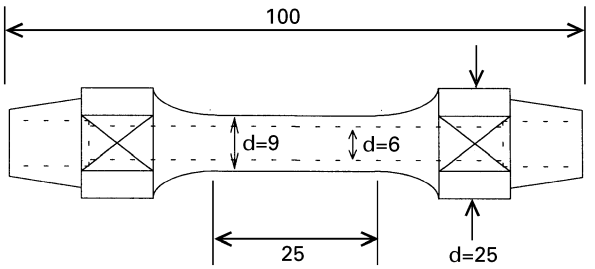

Figure 3 Tubular tension–torsion testpiece.

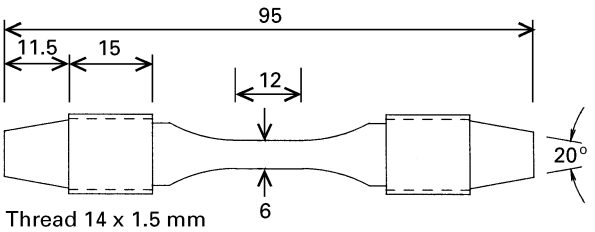

Figure 4 Solid LCF specimen.

Optical and scanning electron microscopy (SEM) were used to examine the physical features of failed specimens. Representative fractures from each alloy were thereby selected for EBSD examination in order to obtain crystallographic orientation measurements of planar facet surfaces and neighbouring grains.

2.2. EBSD techniques

Detailed crystallographic data were obtained in a Jeol scanning electron microscope (JSM 6100) equipped with an EBSD system incorporating a phosphur screen, low light video camera, and high resolution monitor. The methodology of EBSD pattern generation and analysis are well documented in a review by Dingley and Randle [5]. Essentially, a highly focussed

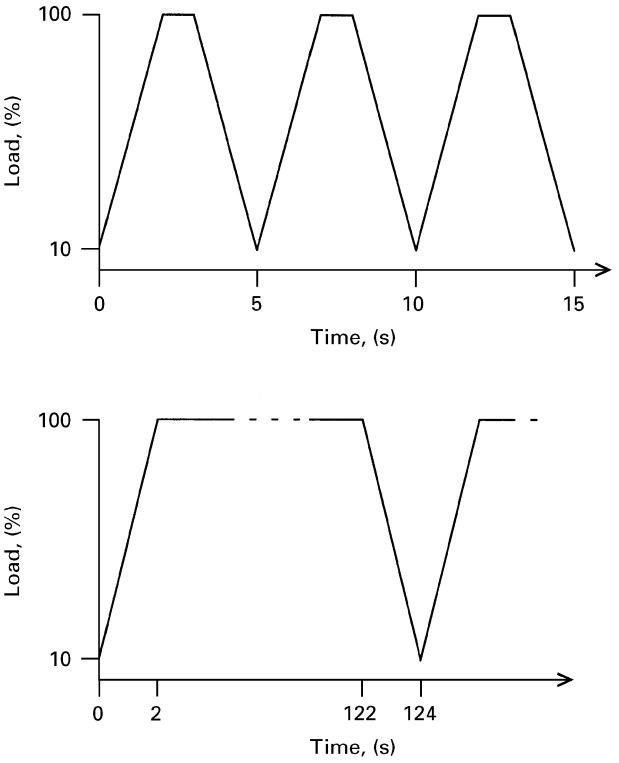

Figure 5 Cyclic (top) and dwell loading waveforms.

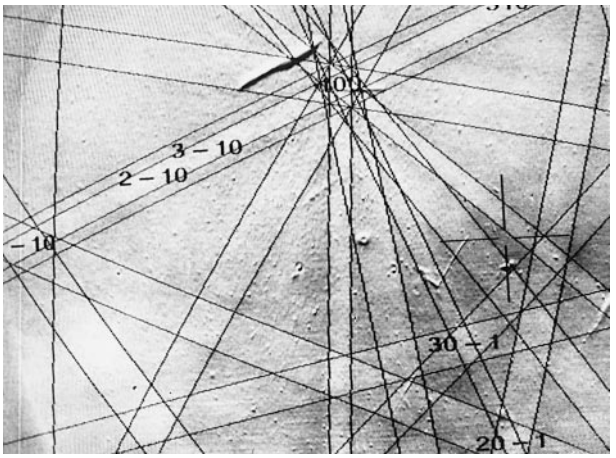

Figure 6 Typical EBSD pattern from IMI685.

primary electron beam strikes an inclined specimen surface supported in the SEM chamber. Due to a small angle of incidence (between 10° and 30°) a large proportion of the electrons are backscattered by the lattice planes in the specimen. These electrons strike a phosphur screen and create distinctive Kikuchi patterns according to Bragg diffraction conditions. A typical example from the present work is presented in Fig. 6. In the present case, the patterns were analysed using a computer software package which includes real time imaging and background subtraction image enhancement. The patterns were indexed via the computer to calculate the crystallographic orientation of the selected region. The orientation data are then presented as inverse pole figures.

In practice, the electron beam penetrates a surface layer approximately 10 nm in depth. It is essential that this layer is relatively strain free and clean. For the IMI685 specimens, this required metallographic sectioning and mechanical polishing at 90° to the features of interest on the plane of fracture. This meant careful positioning and alignment of facets in the case of 60 ppm material and regions of α/β interface cracking in the high hydrogen specimens. The orientation of features on the fracture surface could therefore be inferred from readings taken on orthogonal sections.

Sectioning through the much finer facets on IMI834 proved to be unreliable. Thus the EBSD technique was used directly on the fractured surfaces of these specimens. Specimens were cleaned in an ultrasonic bath containing a surface degreasing solution and lightly etched using Kroll's agent. The electron beam was focussed directly onto the facets. These facets contained similar features to those in IMI685 except much smaller in scale (typically 30–50 μm across compared to a maximum of 1.5 mm in IMI685).

3. Results

3.1. Fatigue response

The cyclic and dwell fatigue data for IMI685 with 60 ppm and 250 ppm hydrogen contents are shown in Fig. 7. Cyclic data for IMI834 with an as received hydrogen concentration of 40 ppm are also included. The applied fatigue stress levels have been normalized by the monotonic tensile strengths of the respective alloys. Table I contains details of the relevant monotonic properties. For cyclic loading, a good correlation is noted between the two different alloys when plotted on this normalized basis. Increased hydrogen levels in the IMI685 induce a weaker fatigue response, especially under dwell loading where lives are reduced by approximately two orders of magnitude compared

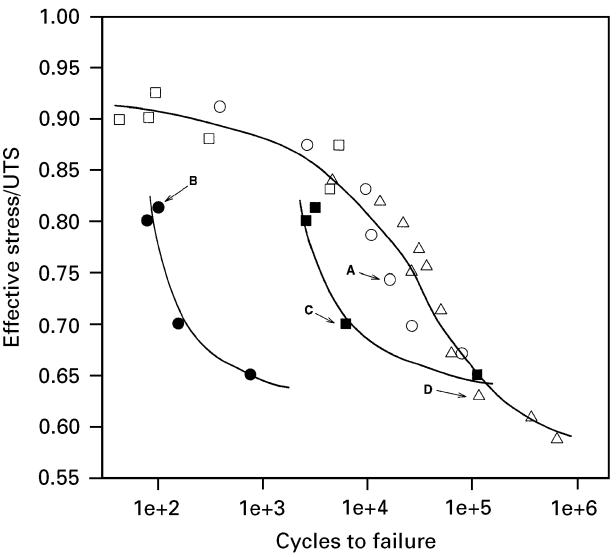

Figure 7 Low cycle fatigue data for IMI685 and IMI834. Data taken for; (○) IMI685 60 ppm cyclic tension/torsion, (□) IMI685 60 ppm dwell tension/torsion, (■) IMI685 > 100 ppm cyclic tension/torsion, (●) IMI685 > 100 ppm dwell tension/torsion and (△) IMI834 cyclic tension.

TABLE I Measured monotonic data for IMI685 and IMI834

Alloy	UTS (MPa)
IMI685 aligned 60 ppm hydrogen	976
IMI685 aligned 250 ppm hydrogen	998
IMI834 bimodal 40 ppm hydrogen	1190

to the 60 ppm material. The specimens selected for subsequent EBSD analysis are indicated by the letters A, B and C for IMI685 and D for IMI834.

3.2. Characterization of facets in material with as received hydrogen contents.

Fracture surfaces in IMI685 displayed characteristic features according to the different hydrogen concentrations. In the as received 60 ppm level, quasi-cleavage facets were commonplace. A single dominant facet orientated approximately perpendicular to the tensile axis was often the site of crack initiation. In one testpiece (specimen A) chosen for EBSD analysis the facet extended across the complete tubular specimen wall section (i.e., 1.5 mm), Fig. 8. Its orientation was confirmed as perpendicular to the tensile loading axis by a series of mounted sections through the facet at intervals of approximately 0.1 mm. An example is shown in Fig. 9 which relates to the position marked A in Fig. 8. The facet surface is remarkably flat. Immediately below the surface individual colonies of aligned alpha plates can be defined, all inclined at roughly 10° to the vertical. Together, these steeply inclined colonies delineate a single grain. Below and notably to the right hand side, neighbouring grains can be identified with aligned colonies of different orientation. A total of forty EBSD readings were taken from this section at random positions within 300 μm of the facet surface. The majority of the measurements are illustrated in the corresponding inverse pole diagram of Fig. 10. They demonstrate that the polished section of the grain in which the facet has developed is orientated at 80° to 90° away from the basal plane. Further, it is well established [6] that α platelets are orientated such that the α/β interfaces lie parallel to the *C* axis of the hexagonal lattice, with the interfaces lying on or close to the {1 0 1 0} prismatic planes. Therefore, it can be deduced that the

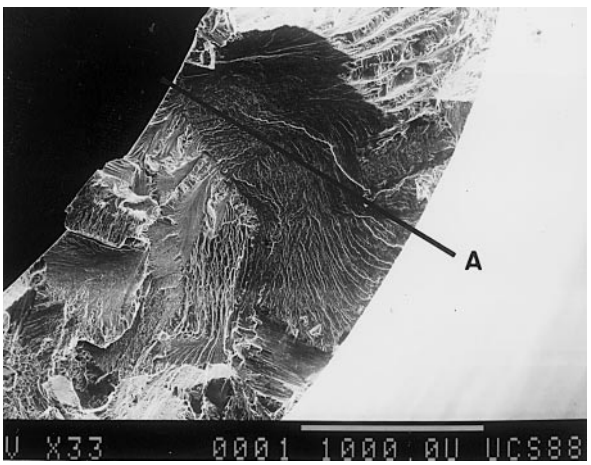

Figure 8 Facet developed in IMI685 containing 60 ppm hydrogen. (Section A refers to Fig. 9).

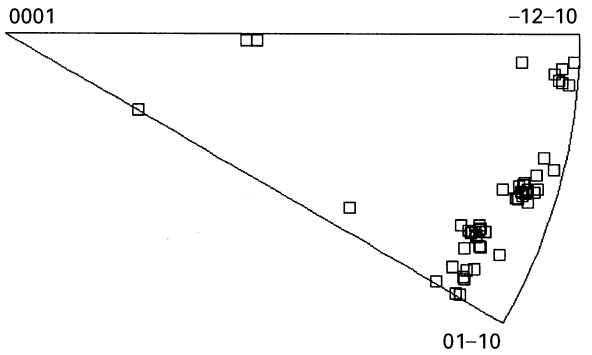

Figure 10 Inverse pole diagram for EBSD readings taken from the section through a 60 ppm facet (Fig. 9).

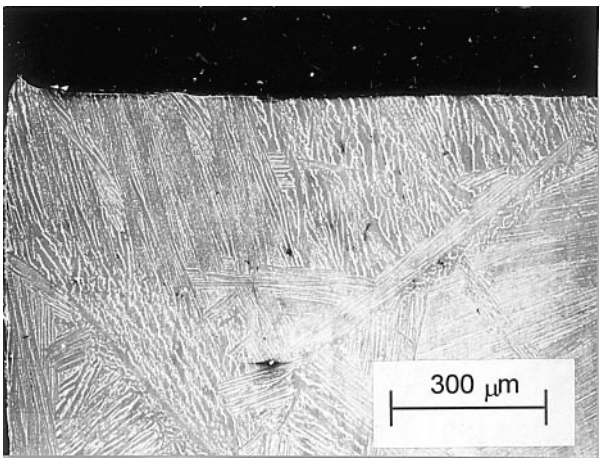

Figure 9 Vertical section through the facet illustrated in Fig. 8.

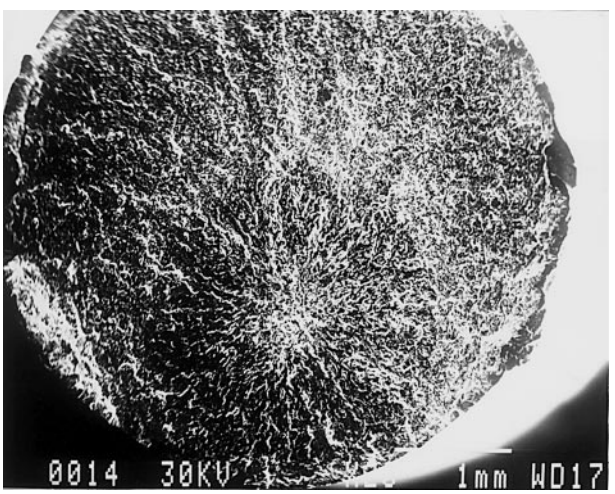

Figure 11 Sub-surface initiated failure in IMI834.

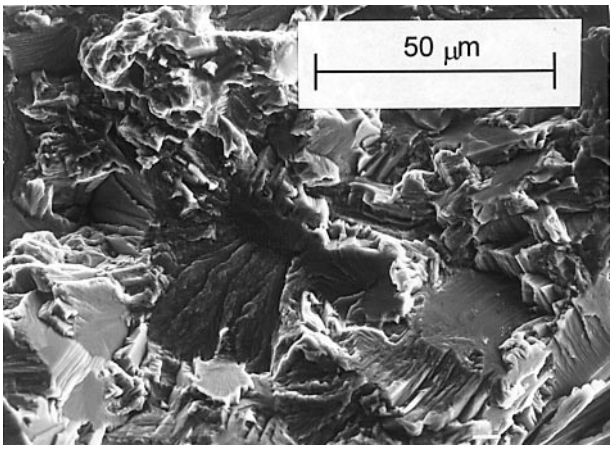

Figure 12 Facets at the initiation site in IMI834.

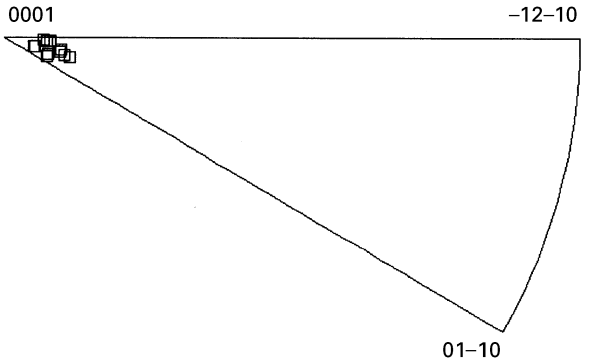

Figure 13 Inverse pole diagram for EBSD readings taken directly from facets on a fracture surface in IMI834.

facet plane has a near basal orientation. Any readings suggesting a different orientation were related to the orientation of neighbouring grains in Fig. 9.

Sub-surface initiated failures are commonplace in IMI834, Fig. 11. At the origin of these sites, facets occur which are similar in appearance to those in IMI685. However, due to the much finer microstructure for IMI834, these were more numerous and notably smaller in scale, Fig. 12. For this example (specimen D), EBSD patterns were successfully analysed directly from the facet surface without the need for prior sectioning. The resultant pole figure confirms a near basal orientation for these facets, Fig. 13. Similar measurements, direct from large facets on the fracture surfaces of IMI685 specimens, have also confirmed their near basal plane orientation.

3.3. Fractures in IMI685 with >100 ppm hydrogen content

Fracture surfaces in high hydrogen testpieces were notably different. In particular, there is significant cracking along alpha–beta interfaces and at prior beta grain boundaries. There is also evidence of basal plane fractures but these appear to act as a link between the interface/boundary cracking. Fig. 14 shows a typical cross-section from a torsion dwell failure (specimen B). The crack path is characteristically helical with respect to the specimen axis. However, within

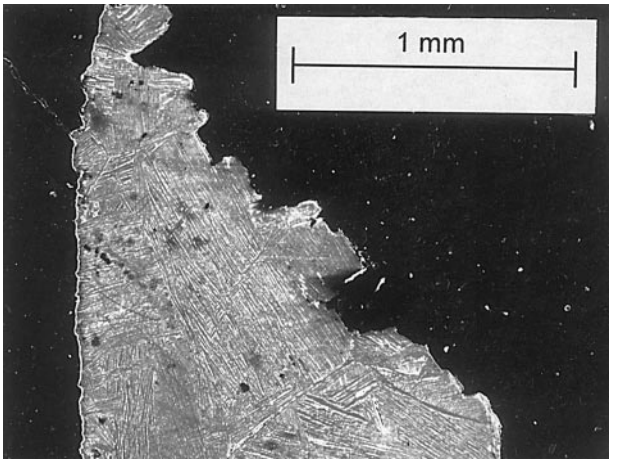

Figure 14 Cross-section of a high hydrogen fracture in IMI685 under dwell torsion, $\sigma_{\text{eff}} = 812$ MPa.

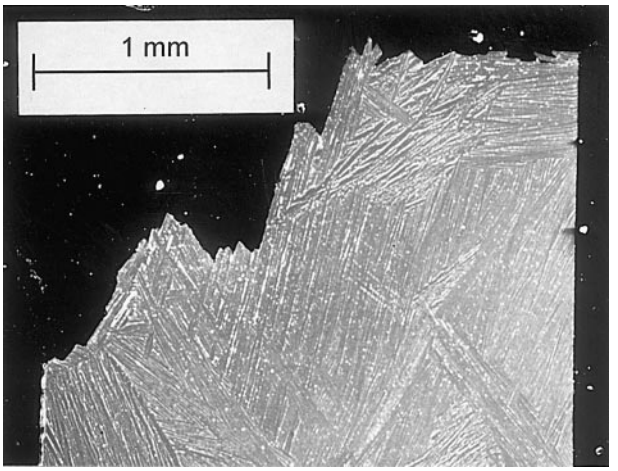

Figure 15 As Fig. 14 except under cyclic tension, $\sigma = 750$ MPa.

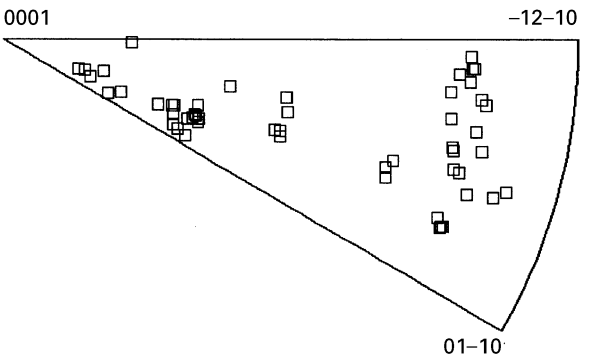

Figure 16 Inverse pole diagram for EBSD readings taken from the section through a IMI685 high hydrogen cyclic tension failure.

this general trend there are considerable deviations. In the case of cyclic tension (specimen C), it is clear that the microstructure and in particular the α/β interfaces play a dominant role in determining the fracture path, Fig. 15. The inverse pole figure from this section is shown in Fig. 16. The readings were taken from random positions just beneath the fracture surface and across the whole of the exposed section. It is clear that the preferred basal texture of the 60 ppm facetted

features is not repeated. Fig. 17 focusses more precisely on the fracture path by examining a small sub-crack away from the main path in a torsion specimen. Fig. 18 is a pole figure for the area around this sub-crack. It is emphasised again, that the points relate to the orientation of normals to the polished surface. By inference, however, the regions marked 35, 36 and 37 suggest there is a basal plane at right angles to the surface. The orientation of the aligned structure

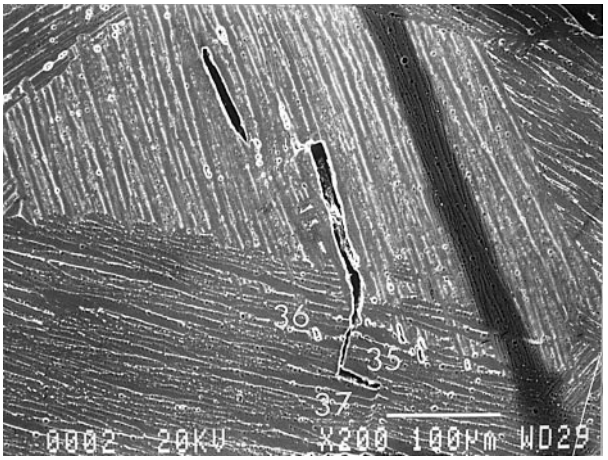

Figure 17 Localised sub-crack in a high hydrogen fractured test-piece.

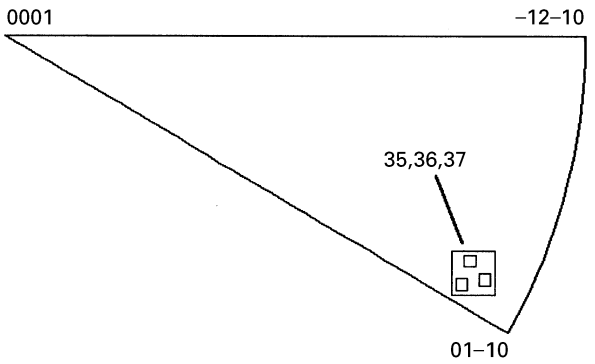

Figure 18 Inverse pole diagram for EBSD readings taken from the region of the sub-crack in Fig. 17.

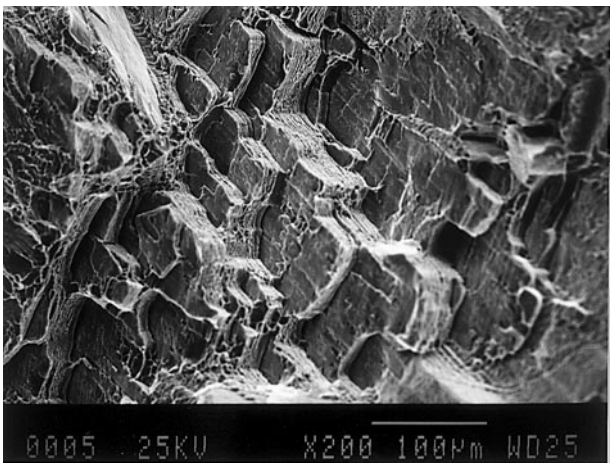

Figure 19 Fracture surface features for a high hydrogen failure in IMI685.

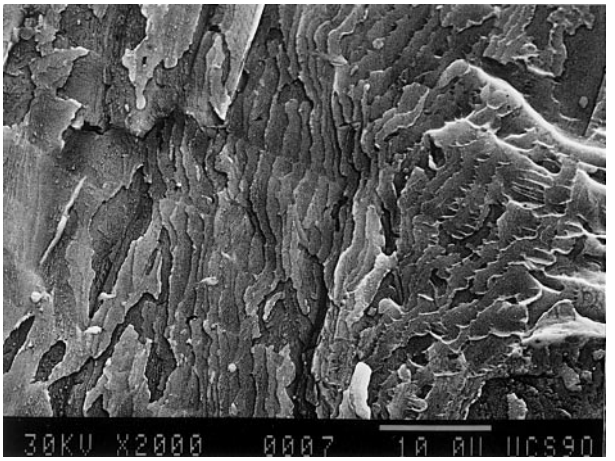

Figure 20 Terrace features formed by α/β interface cracking in IMI685 with high hydrogen.

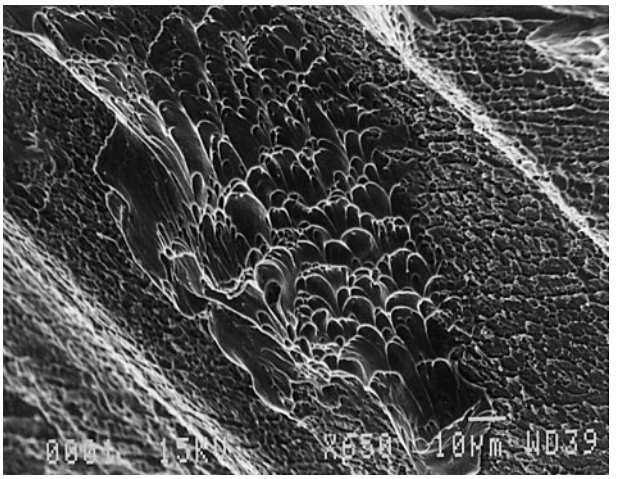

Figure 21 Ductile voids on a basal plane in IMI685 with high hydrogen.

further indicates that this plane must lie in a near vertical direction.

Examinations of the fracture surfaces are consistent with the metallographic sections and with the deductions from the EBSD analysis. Thus there is evidence of α/β interface cracking, grain boundary separation and propagation across basal planes, Fig. 19. At higher magnifications, the interfaces show evidence of terraces, Fig. 20, while on the basal planes there are ductile voids which have an elongated morphology, Fig. 21.

4. Discussion

It has been previously reported that the response of IMI685, containing different levels of interstitial hydrogen, to both monotonic and fatigue loading provides an important insight into the mechanisms of facet formation in titanium alloys [1, 3, 7]. The data from different hydrogen levels give a progressive and consistent pattern of behaviour. Monotonic stress–strain curves demonstrate an increase in both yield and ultimate failure strength as the hydrogen content increases. However, this change is accompanied by a decrease in ductility. The clear indication

is that hydrogen atoms modify dislocation behaviour, particularly at lower concentrations, but then above a critical level (i.e., 100 ppm in IMI685) they induce additional failure mechanisms. This assumption is bourne out by the examination of the fractured test-pieces with different hydrogen concentrations during the present study.

For a hydrogen content of 60 ppm, a single dominant facet is usually found at the site of crack initiation, particularly if the magnitude of applied cyclic stress is relatively low i.e., between the cyclic and monotonic yield strengths. Under such conditions the facets are normally perpendicular to the tensile stress axis, Figs. 8 and 9. After a process of sectioning and polishing, EBSD analysis has reinforced the view that these facets have a near basal plane orientation with respect to the hexagonal crystal lattice. This observation is consistent with the work of Davidson and Eylon [2]. For near alpha titanium alloys at ambient temperature the basal plane is associated with dislocation movement. However, it is clear from Fig. 9 that these planes are perpendicular to the applied stress and not favourably orientated for slip. Nevertheless, the work of Wojcik *et al.* [8] shows that facet formation requires a critical combination of shear stress (i.e., basal slip) and tensile stress normal to the slip plane. In the present case, the facets have obviously developed on a plane where the normal stress is high. A model has recently been proposed to show how this critical combination of tension and shear can be met [1]. It argues that slip bands in grains adjacent to the poorly orientated basal plane can induce the required shear stresses for facet formation. Clearly stress redistribution is important in this highly anisotropic microstructure.

It has been further demonstrated that the EBSD technique can also be applied to the much finer facets in IMI834. This compliments the findings of Sarrazin *et al.* who achieved similar success with EBSD analysis on a Ti–6Al–4V alloy [9]. It is particularly significant that the diffraction patterns were obtained directly from the fracture surface. This was possible because the facets at the sub-surface initiation site were relatively flat and smooth but most importantly, they were orientated approximately perpendicular to the longitudinal loading axis of the specimens. The measurements, Fig. 13, clearly confirm that they are also basal planes. Clearly, the slip band model and stress redistribution are once again important factors in their formation.

The high hydrogen failures in IMI685 provide a contrasting series of failure mechanisms. Basically there are three elements; α/β interface cracking, prior β boundary cracking and separation along basal planes. The interface cracking and basal plane fracture path from a torsion failure are illustrated in Fig. 17. A schematic diagram representing this region is shown in Fig. 22. The shear stress and tensile stress directions are superimposed on the figure. It appears that the interface cracking is associated with the tensile component of stress. The cracking on the basal plane, however, occurs when the plane coincides with the horizontal or vertical shear stress components. It is

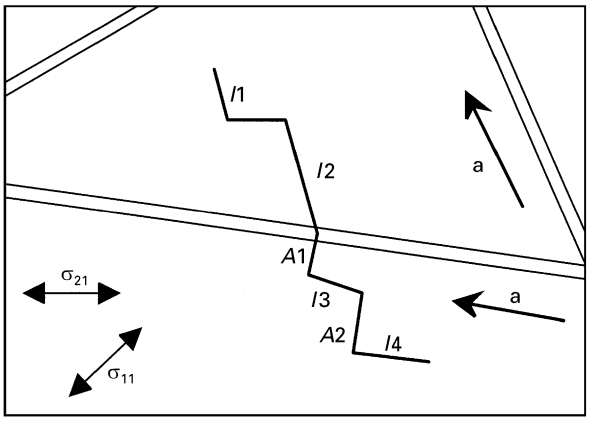

Figure 22 Schematic representation of the sub-crack system in Fig. 17. (=) represents the colony boundary whilst (–) represents the crack path (.1 = interfacial, A = across alignment) a = plate boundary orientation.

instructive to consider the fracture surface features illustrated in Figs. 19 and 20. Where the crack grows along the interface, the fracture surface is comparatively smooth but there is evidence of terraced or arrest features. The smoothness suggests a highly brittle event while the terraces are considered to be related to hydride formation and fracture [3, 4]. It is well established that hydride formation can be associated with the interface regions. When the crack traverses basal planes, the fracture surfaces contain evidence of ductile void formation, Fig. 21. These voids are elongated suggesting a shear mode of deformation which is consistent with the orientation of the basal planes and the shear stress of the loading system. The voids are consistent with the shear localization theories of Birnbaum [10]. It is argued that the hydrogen is distributed inhomogeneously in the matrix. Where concentrated it can enhance plasticity locally. Deformation in these regions is intense even though the overall macroscopic response suggests an essentially brittle response. The build up of shear localisation eventually leads to ductile failure processes as observed here. In previous publications, it has been demonstrated that the high hydrogen fractures in IMI685 are associated with macroscopic strain accumulation [3]. The intriguing aspect of this is that the amount of strain for a given stress ($\sim$0.006 at 750 MPa) is independent of whether dwell or cyclic loading is applied. Furthermore, within the general material scatter the time to achieve this strain is independent of dwell or cyclic waveform. This contrasts significantly with the behaviour at lower hydrogen levels in which both strain and time to failure are dependent on the applied waveform. On the basis of i) these observations, ii) the elongated voids on the basal plane, iii) the relationship of this plane to the shear direction in torsion and iv) the work of Birnbaum, it is tempting to attribute the triggering event in these complex fractures to the separation of basal planes under the action of a shear stress. Once a crack has formed, its stress field would act to induce hydride formation at the interfaces which in turn fracture in directions which are approximately at right angles to the principal stress direction. Generally, these events are competitive but the fact

that hydride formation and strain localisation are evident in the same material is not uncommon and has been reported for α titanium [10].

5. Conclusions

The effectiveness of the EBSD technique for studying fracture behaviour of near alpha titanium alloys has been demonstrated. In particular it has been used to confirm the basal plane orientation of facets in dwell and cyclic fatigue fractures of coarse grained IMI685. Furthermore, it has been applied directly to the much smaller (20 μm) facets observed at sub-surface initiation sites in IMI834 and confirmed their basal plane character. At high hydrogen levels, it has been used to confirm the importance of basal plane deformation and slip localization in the observed premature failures of IMI685. A pattern of events has been suggested which links slip localisation, shear dominated ductile failure and hydride formation at alpha–beta interfaces.

References

1. W. J. EVANS and M. R. BACHE, *Int. J. Fatigue* **16** (1994) 443.
2. D. L. DAVIDSON and D. EYLON, *Met. Trans. A* **11A** (1980) 837.
3. W. J. EVANS and M. R. BACHE, *Scripta Met.* **32** (1995) 1019.
4. *idem* in Titanium '95 Science and Technology Proc. 8th World Conf. on Titanium, 1995, Birmingham, U.K. edited by P. A. Blenkinsop, W. J. Evans and H. M. Flower (Institute of Metals, London) p 1339.
5. D. J. DINGLEY and V. RANDLE, *J. Mater. Sci.* **27** (1992) 4545.
6. D. EYLON, *Met. Trans. A* **10A** (1979) 311.
7. M. R. BACHE and W. J. EVANS, *Int. J. Fatigue* **14** (1992) 331.
8. C. C. WOJCIK, K. S. CHAN and D. A. KOSS, *Acta Met.* **36** (1988) 1261.
9. C. SARRAZIN, R. CHIRON, S. LESTERLIN and J. PETIT, *Fatigue Fract. Engng. Mater. Struct.* **17** (1994) 1383.
10. J. LUFRANO, P. SOFRONIS and H. K. BIRNBAUM, *J. Mech. Phys. Solid* **44(2)** (1996) 179.

Received 19 April
and accepted 21 May 1996